Occurrence of Warm Freezing Rain: Observation and Modelling Study

Zhengqi Lu[1], Yongxiang Han[1 2*], Yangang Liu [3*]

[1]Collaborative Innovation Center on Forecast and Evaluation of Meteorological Disasters, Nanjing University of Information Science and Technology, Nanjing, 210044, China.

[2]Key Laboratory for Aerosol-Cloud-Precipitation of China Meteorological Administration, Nanjing University of Information Science & Technology, Nanjing, 210044, China

[3]Brookhaven National Laboratory, Upton, NY, USA

Corresponding author: Yongxiang Han (han-yx66@126.com)

Key Points:

- About 7% of freezing rain events occur when the near surface air temperature is above 0℃ (warm freezing rain).
- A theoretical model is developed to explain the occurrence of warm freezing rain.
- Temperature lag of raindrops is the main cause of warm freezing rain and the critical impact factors are raindrop sizes, lapse rate, and relative humidity.

Abstract

Freezing rain has been normally considered to be composed of supercooled raindrops when the near surface air temperature is below freezing. However, according to a statistical survey of freezing rain events in China over the last two decades (from 2000 to 2019), we find that there were 656 cases occurring at near surface air temperature greater than 0℃ (hereafter warm freezing rain and denoted by WFR), which account for 7% of the total freezing rain events. To explain this phenomenon, a theoretical model is established by relaxing the equilibrium assumption to consider the transient heat exchange between raindrops and the surrounding atmosphere. Sensitivity analysis of the model shows that the temperature lag of raindrops to atmosphere is the main cause of WFR. The direction of raindrop temperature departure from the equilibrium depends on the sign of the temperature lapse rate , and the magnitude of the temperature lag is determined by the raindrop diameter D, , and relative humidity RH. An increase of D, an increase of , and a decrease of RH enhance the lag of raindrop temperature and thus the occurrence of the WFR events. Further simulations of 4 ideal and 25 real sounding profiles reveal that WFR events can form by

the "melting of solid hydrometeors" or "supercooled warm rain process" when considering the temperature lag between raindrops and the atmosphere. With the assumption of initial raindrop diameter of 2mm, together the observed and RH, the model can diagnose more than 95% of WFR events.

1 Introduction

Freezing rain is supercooled precipitation near the surface, i.e., raindrop temperatures are below 0℃, posing one of the major winter weather hazards in countries such as Canada, Sweden, Russia, and China (Adhikari and Liu, 2019; Andersson and Chapman, 2011; Cortinas et al., 2004; Deng et al., 2012). Long-term persistence of freezing precipitation can not only damage the electricity system, transportation, and public infrastructure by causing tower collapses, line freezing, and poor communication, but also result in economic losses and human casualties (Kiessling et al., 2014). For example, from January to February 2008, a long-term and wide-ranging freezing rain event occurred in southern China that caused direct economic losses of ¥150 billion (Zhao et al., 2008). Therefore, studies on the microphysical processes of freezing rain can deepen our understanding of the formation mechanism of freezing rain and provide an important scientific basis for accurate freezing rain forecasting and thus reduce economic losses caused by freezing rain.

Numerous studies have been conducted on the formation process of freezing rain and two microphysical mechanisms have been proposed: "melting mechanism" (Rauber et al., 1994; Tobin and Dana, 2017) and "supercooled warm rain mechanism" (Huffman and Norman, 1988; Roberts and Stewart, 2008; Stewart et al., 2015). In the "melting mechanism", snow or ice crystals formed in the upper air melt completely into raindrops as they fall through a warm layer (temperature >0℃). Subsequently, the raindrops fall into a sub-freezing layer (<0℃) and become supercooled raindrops (Rauber et al., 1994). In the "supercooled warm rain mechanism", freezing rain grows by collision and coalescence of supercooled cloud droplets and raindrops (Huffman and Norman, 1988), and the air temperature is maintained below 0℃ as the raindrops fall. Based on these two mechanisms, several parameterization schemes have been developed to constrain the phase transformation in the formation of freezing rain (Hindmarsh et al., 2003; Milbrandt and Yau, 2005; Gibson and Stewart, 2007; Stewart et al., 2015; Nagumo et al., 2019), including the transient melting scheme (Thompson et al., 2008), thermodynamic melting scheme (Sanders and Barjenbruch, 2016) for ice crystal melting processes, and the refreezing process (Johnson and Hallett, 1968) for mixed-phase precipitation. Cyzs et al. (1996) established a diagnostic model based on the "melting mechanism" of freezing rain. In this model, the freezing rain is determined when snowflakes or ice crystals have completely melted in the melting layer and fall into the sub-freezing layer near the ground. By adding the prognostic equation for the liquid fraction of mixed-phase particles to the bulk microphysics scheme (Morrison and Grabowski, 2015), Cholette et al. (2020) developed a new scheme to reduce the overestimation of freezing rain rate. Hanesiak and Stewart (1995) suggested that supercooled raindrops

in the refreezing layer would refreeze through collision with ice crystals, and thus reduce the amount of freezing rain near the ground. Barszcz et al. (2018) added this microphysical process to Canada's 2.5-km numerical weather prediction model and significantly improved the accuracy of freezing rain forecasting.

These studies provide theoretical support for the formation of freezing rain. However, all these studies are based on the assumption that freezing rain forms when the near-surface air temperature (hereafter surface temperature for convenience) is below 0℃, indicating that surface temperature below 0 °C is necessary for freezing rain formation.

Furthermore, a review of previous studies on the formation mechanism of freezing rain reveals that all studies assumed the raindrops maintain an equilibrium state and the raindrop temperature (T_r) being equal to the air temperature (T_a) under a saturated atmosphere. However, this is an ideal state. Due to the time scale of changes in the atmospheric conditions is often shorter than the relaxation time scale of raindrops, the raindrop cannot maintain an equilibrium state and the heat budget of raindrops is unbalanced when they fall into the real atmosphere (Tardif and Rasmussen, 2010). Therefore, the variation of T_r always lags that of T_a (Caplan, 1966; Gosnell et al., 1995, Wu, 1991). Some observational studies have verified this theory. For example, the observational study by Anderson et al. (1998) showed that the difference between T_r and T_a is at least 0.4℃ when raindrops are falling. Further studies (Lee and Feingold, 2010; Khain et al., 2011; Salamalikis et al., 2016) showed that the difference between T_r and T_a depends on many factors, including season, time of day, and other meteorological conditions.

In this study, we first analyze the freezing rain events observed in China over the last two decades (from 2000 to 2019). A total of 9,312 freezing rain events is identified, 93% of which could be explained by the two formation mechanisms mentioned above; however, 7% (656 cases) of the freezing rain events occurred when the surface temperature was >0 °C. We refer to this phenomenon as warm freezing rain (hereafter WFR). Some researchers have noticed this phenomenon (Cortinas et al., 2004), but the WFR formation has never been further studied and represented in the freezing rain parameterization. According to our research, WFR events occur frequently and are distributed across different regions. Furthermore, neither the "melting" nor the "supercooled warm rain mechanism" can explain WFR events, which implies that some unknown mechanism(s) is missing. To explain the WFR events, we then present a theoretical model by relaxing the equilibrium assumption of T_r to consider the transient heat exchange between raindrops and the ambient atmosphere. Several sensitivity studies are further conducted with this model to examine the effects on T_r of key meteorological variables including raindrop diameter, temperature lapse rate, and relative humidity. Finally, WFR formation and the corresponding meteorological conditions are discussed.

2 Observational analysis

The observation data are obtained from the China Meteorological Administration (CMA). It includes radiosonde data from 89 sounding stations across China at 00:00 and 12:00 UTC, and surface temperature, dew-point temperature, and weather phenomena data at 2,168 ground stations at 00:00, 06:00, 12:00, and 18:00 UTC from January 2000 to December 2019. These data were subjected to quality control and homogeneity tests by the CMA (Zhou, 2000). The spatial distribution of the sounding and ground stations is shown in Figure 1.

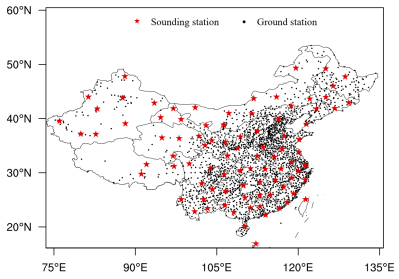

Figure 1. Distribution of sounding stations (stars) and ground stations (dots) in China.

Figure 2a shows the frequency distribution of the surface temperature when freezing rain events occurred at the ground stations in China from 2000 to 2019. A total of 9,312 freezing rain events were observed over the 20-year period, 90% (8,394) of which occurred when the surface temperature was between -6 and 0 °C. This statistic is consistent with the results of Cortinas (2004) and Zhou (2017). However, nearly 7% (656) of the freezing rain events occurred when the surface temperature was higher than 0 °C. The frequency of such WFR events gradually decreases as the surface temperature increases, but they can still occur at surface temperatures > 1 °C (Figure 2b).

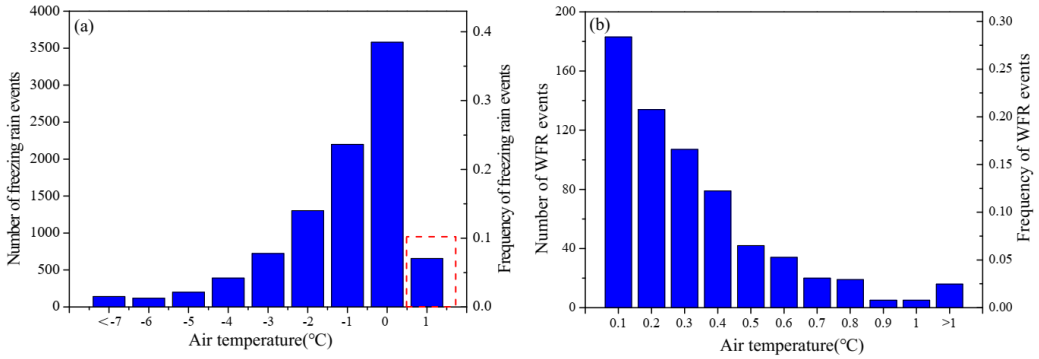

Figure 2. Occurrence frequency of freezing rain (a) and warm freezing rain (b) as a function of surface temperature. The observations were from 2000 to 2019.

Some observational studies have shown that the meteorological characteristics and formation mechanisms of freezing rain change with station altitudes (Carrière et al., 2000). To examine whether the station altitude affects the formation of WFR events, the frequency and proportion of WFR events at stations with different altitudes are analyzed. The results show that the frequency of WFR events decreases with increasing station altitudes (Figure 3). Over the entire study period, 360 WFR events were observed at ground stations with station altitudes between 0 and 500 m, accounting for 18% of the total number of freezing rain events in this station altitude range. The ground stations at altitudes >2000 m only observed 41 WFR events, representing 3% of the total number of freezing rain events at this station altitude. It is obvious that the frequency and proportion of WFR events occurring at low station altitudes are significantly higher than at high station altitudes, which implies that the station altitude has a significant impact on the spatial distribution of WFR events.

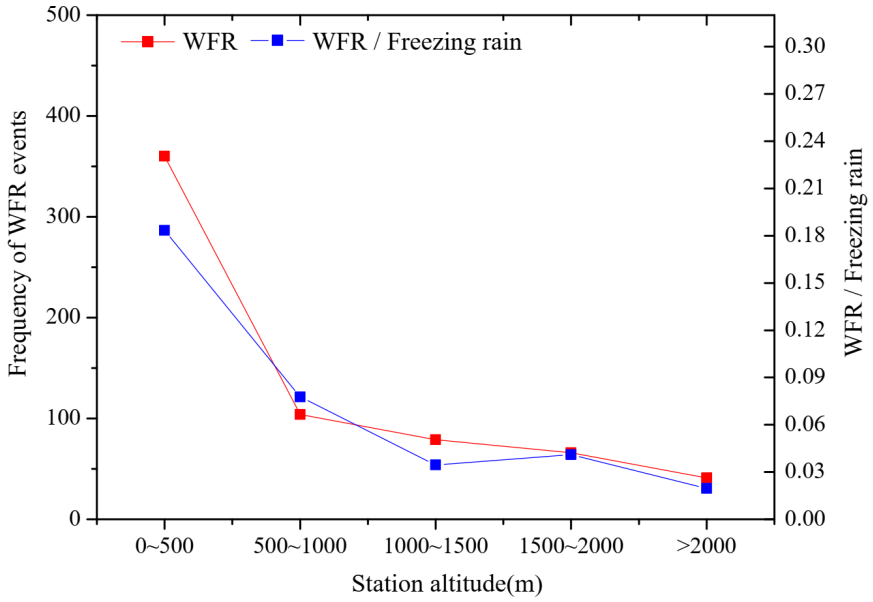

Figure 3. Dependence of frequency and proportion of WFR events on the station altitude of the observational weather stations.

The formation mechanism of freezing rain is closely related to the vertical profile of atmospheric temperature. A total of 25 vertical profiles with WFR have been observed at sounding stations in China (table omitted). Although all of these profiles contain a melting layer or a liquid cloud(cloud top temperature > -10℃), their surface temperature is greater than 0℃. Thus, neither of the "melting mechanism" and "supercooled warm rain mechanism" can explain the WFR events occurring at surface temperatures >0 °C, calling for new and different explanations.

3. Theoretical model and sensitivity studies

3.1. Model

To quantitatively investigate the formation of WFR events, a theoretical model for describing T_r is presented here, but relaxing the equilibrium assumption and considering the radiation, convection and evaporation heat exchange between raindrops and the atmosphere. The model includes some simplifying assumptions used in previous studies (Smorodin et al., 2014; Tardif and Rasmussen, 2010; Caplan, 1966). First, raindrops are assumed to be spherical with a uniform temperature from the drop center to the surface. Second, the raindrop does not grow by the collision-coalescence process during their falling from the cloud base.

The total heat of the raindrops (Q_T) is determined by the heat transfer between raindrops and atmosphere by evaporation (Q_e), convection (Q_h) and radiation (Q_r), which can be described by the following equation (Abraham et al., 1972).

,

Where the components can be expressed as (Pruppacher and Klett, 2012):

,

,

,

Based on the equations (1) ~ (5), the temporal change rate of T_r is described by

In addition, the raindrop fall velocity $U(D)$ can be estimated from (Best, 1950; Atlas et al., 1973):

,

The variables, symbols and empirical parameters in the above equations are summarized in Appendix.

If the particles are solid, the parameterization scheme proposed by Zerr (1973) is used to calculate the melting rate of solid/mixed particles. The initial height of raindrop generation is defined as the height at which solid particles completely melt.

3.2 Sensitivity experiments

In fact, the atmospheric conditions surrounding falling raindrops are changing, which prevents raindrops from reaching and maintaining a steady equilibrium state instantaneously. In principle, T_r is not equal to T_a when the raindrops are falling in real atmosphere. It is possible that T_r <0 °C while T_a >0 °C when the raindrops are falling to the ground, thus resulting in WFR. To better understand the formation mechanism of WFR and explain the frequency distribution of the WFR events, the following sensitivity experiments are conducted.

3.2.1 Experiment design

To simplify the sensitivity study, the model is constrained with the following conditions: 1) The top of the model is set at 1km height, based on the fact that the cloud base height of winter precipitation is usually less than 1 km (Zhang et al., 2018); 2) T_r is equal to T_a when the raindrops start to fall from the 1km height (Tardif and Rasmussen, 2010); 3) the raindrops remain stable in geometric shape (spherical) and no collision-coalescence process occurs among raindrops during falling. 4) hydrostatic atmosphere and surface pressure of 1013.25 hPa are assumed for the atmospheric pressure profile and. The near-surface temperature is set as 0.5℃.

According to the theoretical model of T_r presented in section 3.1, the evaporation, convection and radiation heat transfer of the raindrops and thus T_r are affected by the initial raindrop diameter D, temperature lapse rate Γ and relative humidity RH. Therefore, 3 sensitivity experiments are further conducted (Table 1) to explore the sensitivities in addition to the control experiment. Briefly, the control experiment is to investigate the variation feature of T_r when the raindrops fall from 1km height to the ground by fixing D, Γ and RH at the default values of 2 mm, 80%, and 5 °C/km, respectively. Experiment 1 is to examine the sensitivity to D by fixing Γ, RH at their default values and varying D from 0.5 mm to 4 mm with a diameter interval of 0.1 mm. Experiment 2 is to examine the sensitivity to Γ by fixing D, RH at their default values but varying Γ from -10℃/km to 10℃/km with an interval of 0.5℃/km. Experiment 3 is to examine the sensitivity to RH by fixing t D, Γ at their default values but varying RH from 50% to 100% with an interval of 5%.

Table 1. Sensitivity experiment design.

	Sensitivity parameter	Variation range	Defaul value
CTRL	/	/	D=2mm; Γ=5℃/km; RH=80%;
Ex 1	D	0.5~4mm	RH=80%;Γ=5℃/km;
Ex 2	Γ	-10~10℃/km	D=2mm; RH=80%;
Ex 3	RH	50~100%	D=2mm;Γ=5℃/km;

(CTRL and EX refer to the controlled experiment and sensitivity experiment, respectively.)

3.2.2 Results

3.2.2.1 Control experiment

Figure 4a shows the variations of T_r and T_a with height as a raindrop D = 2 mm falls from 1km height in an atmosphere of RH = 80% and Γ= 5 °C/km. The raindrop reaches the quasi-equilibrium state when they fall 67m (define as the equilibrium distance) from the model top. Before the raindrop reaches the quasi-equilibrium state, the variation rate of T_r is negative and the difference between T_r and T_a (define as the temperature lag, T_{ar}) increases rapidly with the falling distance. The variation rate of T_r drops to 0 and T_r drops to the lowest when the raindrops reach the quasi-equilibrium state. After that, T_r gradually increases with the falling distance and its variation rate is slightly less than that of T_a, which makes the temperature lag of raindrops gradually increase with the falling distance.

To explain the variation of T_r with falling distance, Figure 4b shows the changes in the total heat of the raindrop (Q_T), latent heat of evaporation(Q_e), sensible heat of convection(Q_h) and radiation heat (Q_r) between the raindrop and atmosphere with falling distance. From cloud base to the equilibrium distance, Q_e is much greater than Q_h and Q_r, and the total heat change of raindrop is negative

due to the strong raindrop evaporation. Therefore, the variation rate of T_r is negative and the temperature lag of raindrops rapidly increases with the falling distance. With the increase of T_{ar}, rapidly increases and Q_e decreases with the falling distance. When Q_h is sufficient to compensate for Q_e, T_r reaches the equilibrium temperature of the raindrop (Tardif and Rasmussen, 2010). After that, the raindrop gradually deviates from equilibrium (Tardif and Rasmussen, 2010) since the time scale of change in T_a is shorter than the relaxation time scale of raindrop, resulting in the variation rate of T_r slightly lagging behind that of T_a and the lag term gradually increases with the falling distance. Furthermore, Q_r is much less than Q_e and Q_h and can be neglected in the analysis.

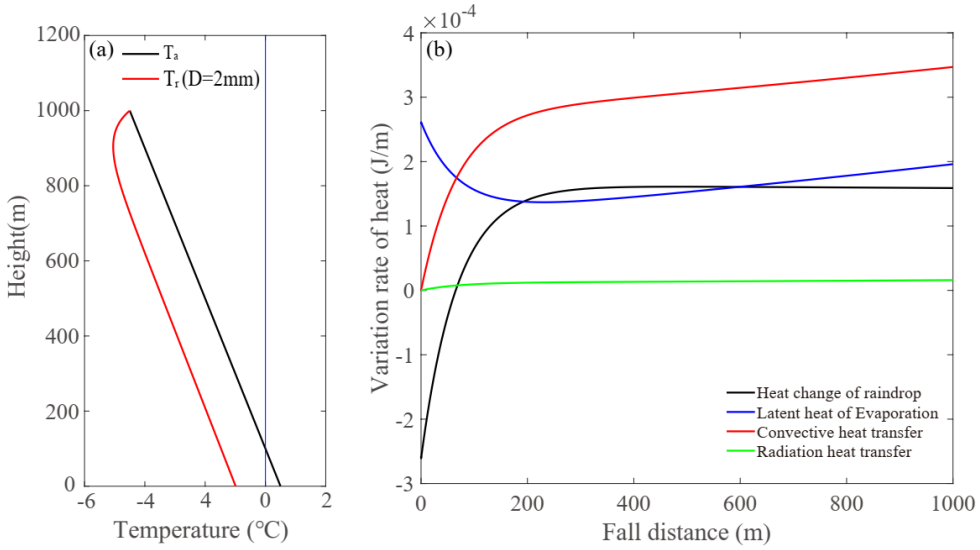

Figure 4. (a) Variation of T_r and Ta with falling distance for the raindrop; (b) Variation of Q_T, Q_e, Q_h and Q_r with falling distance

3.2.2.2 Effect of Raindrop diameter

Figure 5a shows the influence of different raindrop diameters on T_r. As can be seen from Figure 5a, D largely influences the equilibrium distance of raindrops. Until the raindrops reach the quasi-equilibrium state, a larger D leads to a decrease in the variation rate of T_r and a gradual increase in the equilibrium distance of raindrops. For example, the equilibrium distance is only 33m for small raindrops (D=1mm), while it increases to 91m for large raindrops (D=4mm). Furthermore, the temperature lag of raindrops increases with increasing D when the raindrops fall beyond the equilibrium distance.

Figure 5b shows the variation of the T_{ar} for different values of D when the raindrops reach the surface. The results show that T_{ar} is linearly proportional to D, a 1 mm increase in D leads to a rise of 0.4 °C in T_{ar}. This phenomenon is due to smaller raindrops having a larger surface-to-volume ratio and faster

heat transfer between their surface and the atmosphere.

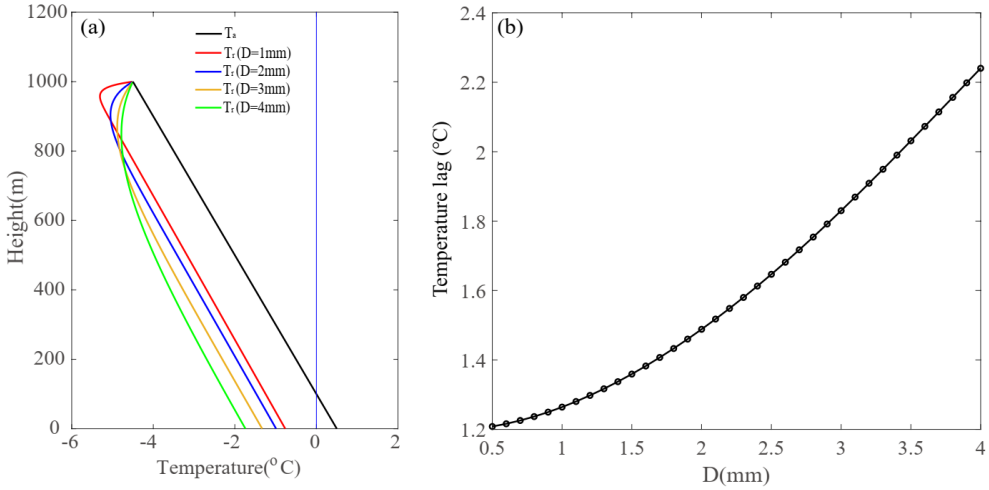

Figure 5. (a) Variation of T_r with falling distance for raindrops of various initial diameters; (b) Variation of T_{ar} with the raindrop diameter D when it falls to the surface.

3.2.2.2 Effect of temperature Lapse rate

Figure 6 shows the effect of Γ on the variation of T_r with falling distance at three different values of Γ. Regardless of the value of Γ, T_r is less than T_a ($T_{\mathrm{ar}} > 0$) until the raindrop reaches the equilibrium state. After that, when Γ is less than 0 ℃/km (Figure 6a), the cooling rate of T_r is lower than that of T_a and T_r gradually deflects to the side of T_a, which means that T_{ar} decrease with the falling of raindrops. When Γ is equal to 0 ℃/km (Figure 6b), T_{ar} varies little with height after the raindrop reaches the quasi-equilibrium state. When Γ is greater than 0 ℃/km (Figure 6a), the heating rate of T_r is slower than that of T_a and results in T_{ar} increase with the falling distance (Figure 6c). This phenomenon shows that the sign of Γ determine the direction of T_r departure from equilibrium.

To further understand the influence of Γ on T_{ar}, Figure 6d shows the variation characteristics of T_{ar} with Γ when the raindrops fall to the surface. The results show that T_{ar} is linearly proportional to Γ, and T_{ar} increases by 0.055 °C for each increase of 1 °C/km in Γ, indicating that the magnitude of Γ determines the degree of deviation of T_r from the atmospheric temperature. Due to the relaxation time scale of raindrops is longer than the time scale of changes in T_a , the cooling/warming rate of T_r is slower than that of T_a. Thus, T_{ar} gradually increases with increasing Γ.

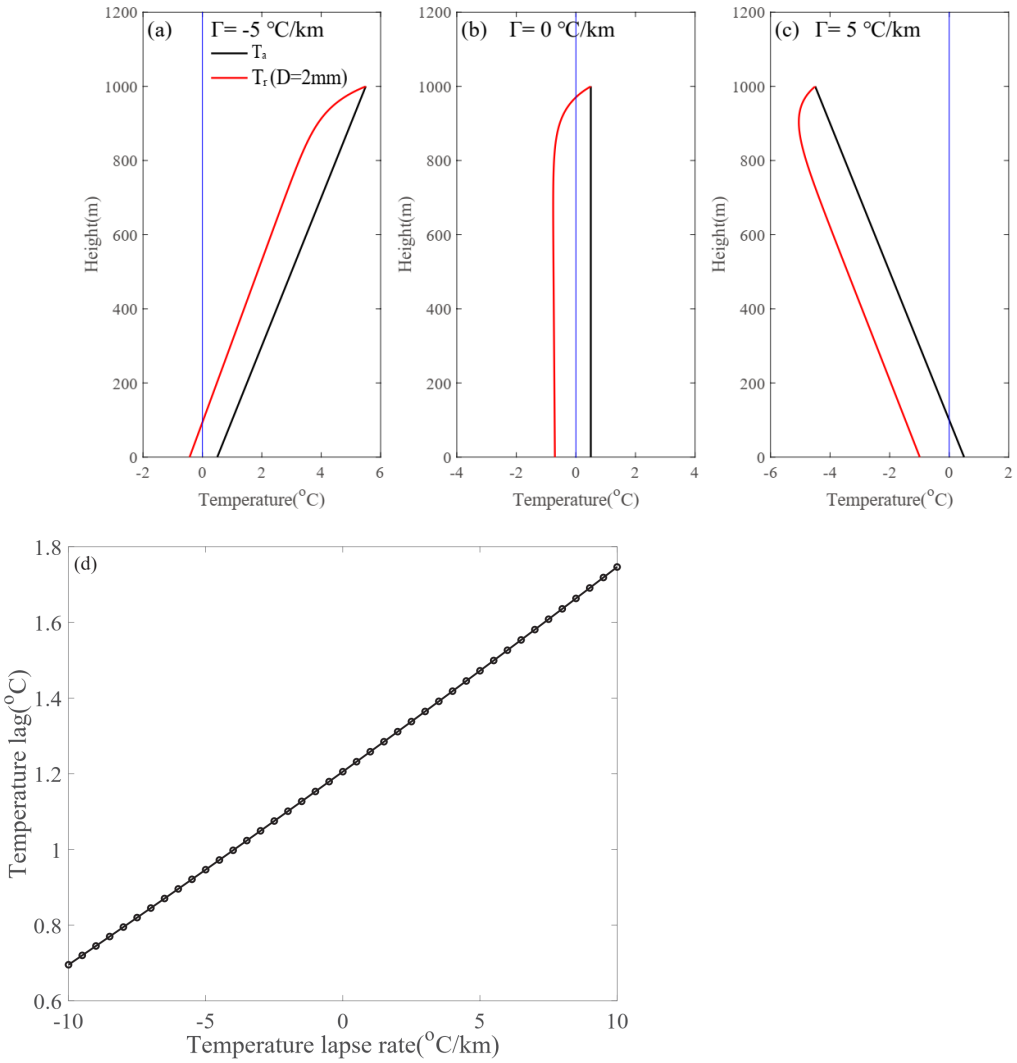

Figure 6. (a-c) Variation of T_r and Ta with falling distance for different three typical values of Γ; (d) relationship between T_{ar} and Γ when the raindrops reach the surface.

3.2.2.3 Effect of Relative humidity

It is well known that RH influences T_r by affecting the evaporation process of the raindrops (Caplan, 1966). As expected, Figure 7a shows that the RH largely influences the variation of T_r with falling distance, a larger RH leads to a decrease in the variation rate of T_r. Figure 7b shows the variation of the T_{ar} at surface is inversely proportional to RH because a larger RH retards the raindrop evaporation process. A larger RH also leads to a smaller T_{ar} required

for the raindrop to reach the equilibrium state. When RH increases from 50% to 100%, T_{ar} decreases from 3.5 ℃ to 0.5 ℃. The result also indicates that the influence of RH on T_{ar} is greater than that of D and Γ.

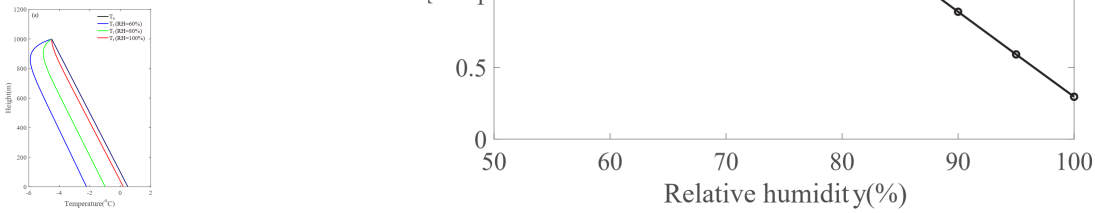

Figure 7. (a) Variation of T_r with falling distance for raindrops of various RH; (b) Variation of T_{ar} at surface with the RH.

3.2.2.4 The combined effect of D, Γ, and RH

The above sensitivity experiments demonstrate that D, Γ, and RH all affect T_r and T_{ar}. The combined effect of the three parameters on T_{ar} can be summarized in Figure 8. On the one hand, the effect of D on T_{ar} depends on the sign and magnitude of Γ. When Γ<0 (ambient temperature increases with height), T_{ar} decreases with D, and T_{ar} becomes more sensitive to D with decreasing Γ. Conversely, when Γ>0 (ambient temperature decreases with height), T_{ar} increases with D. The larger Γ is, the more sensitive T_{ar} is to the change in D. For example, when Γ=-10℃/km, T_{ar} decreases by about 1°C as D increases from 0.5mm to 3mm. When Γ increases to 10°C/km, T_{ar} increases by about 1.5℃ as D increases from 0.5mm to 3mm. This phenomenon implies that when the surface temperature is greater than 0℃, the possibility of WFR is higher for $\Gamma > 0$ than for $\Gamma < 0$. On the other hand, the sensitivity of T_{ar} to RH seems to be unaffected by Γ. Regardless of the sign and value of Γ, T_{ar} gradually decreases with increasing RH.

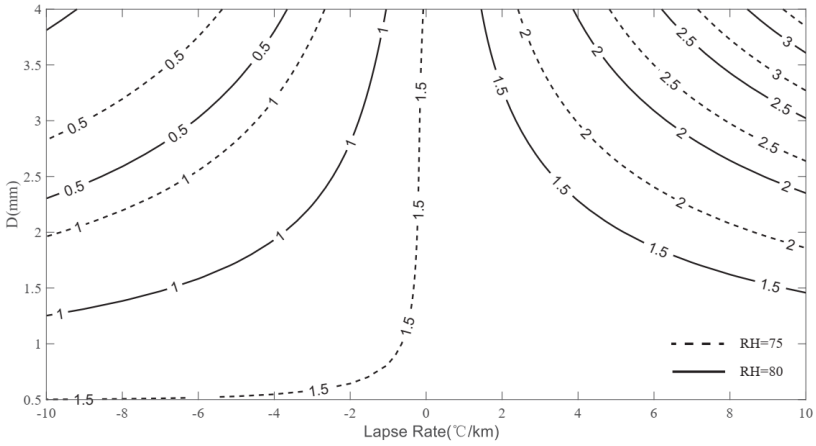

Figure 8. Distribution of T_{ar} for various initial D, Γ, and RH when the raindrops reach the surface (the dashed lines represent T_{ar} when RH=75% and the solid lines represent T_{ar} when RH=80%).

.

3.3 Effect of More Realistic Temperature profiles

The sensitivity experiments have shown that Γ determines the direction and magnitude of T_r departure from equilibrium, thus plays a significant role in the formation of WFR. In the real atmosphere, the temperature profile is composed of multiple values of Γ. For example, winter precipitation is mainly caused by frontal systems that often contain at least one inverse structure in the atmosphere (Thériault and Stewart, 2010). Furthermore, WFR requires the surface temperature greater than 0℃. Therefore, according to the above feature of temperature layers and combinations of different Γ (positive or negative values), four types of ideal temperature profiles are analyzed for the possibility of WFR occurrence (Figure 9). The variations of T_r corresponding to each type of the temperature profiles are calculated (assuming D=2 mm) to determine whether WFR would occur. The first type of profile (Figure 9a) is similar to the "melting mechanisms" profile of freezing rain, including an upper warm layer, a lower sub-freezing layer, and a warm near-surface layer. The calculated result shows that T_r=-1.4℃ when the raindrops fall to the ground. Although the surface temperature is greater than 0℃, the raindrops are still in a supercooled state. Therefore WFR might occur for the first type of profile.

The second and third types of profiles have no sub-freezing layer. Whether the Γ <0 (Figure 9b) or Γ >0 (Figure 9c) in the near-surface layer, T_r is slightly less than 0°C when the raindrops fall into the near-surface layer. Therefore, the possibility of WFR is very less for these two types of profiles.

The fourth profile type (Figure 9d) is similar to the freezing rain profile of the

"supercooled warm rain process", which includes an upper cold layer but a weak warm layer near the surface. The falling raindrops remain supercooled and fall into the weak warm layer with $\Gamma > 0$ near the surface. Due to the temperature lag of the raindrops to the atmosphere, although the surface temperature is greater than 0 °C, T_r near the surface is less than 0 °C (-1.5 °C), which results in WFR.

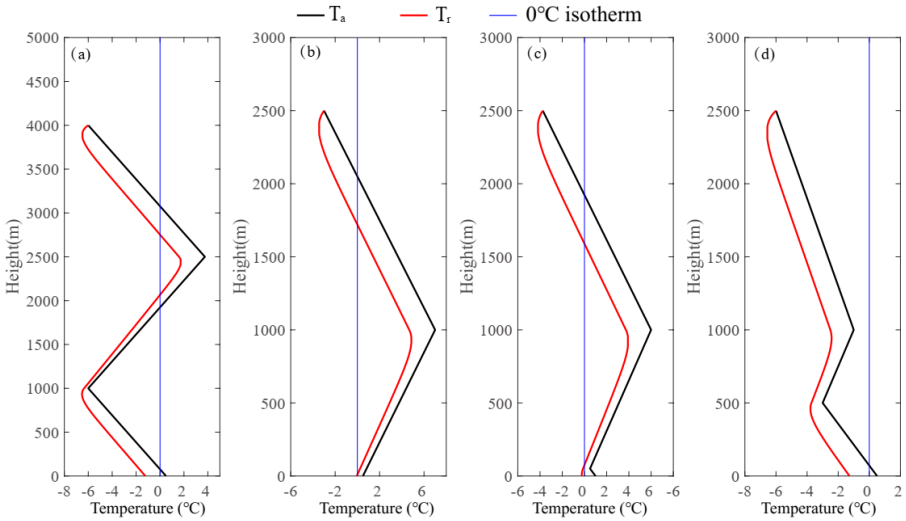

Figure 9. Calculated variations of T_r corresponding to four ideal profiles (D=2 mm).

In summary, the temperature profiles of WFR events have two common features: 1) there is a cold layer (or sub-freezing layer) above the near-surface layer, which allows the raindrops (or completely melted ice crystals) to remain supercooled before falling into the near-surface layer. 2) Γ in the lowest atmosphere needs to be greater than 0℃/km for the raindrops falling into the near-surface layer maintain a large temperature lag with the atmosphere. It is important to note that these results only apply to ideal conditions. In a real atmosphere, the raindrops falling into the cold layer might be coalescing with ice crystals, thus reducing the WFR probability. In general, the first and fourth analyzed profiles have a high possibility for WFR formation.

In addition, the first and fourth profile types correspond to the "melting of solid hydrometors" and the "supercooled warm rain process" for freezing rain, respectively. Although the surface temperatures >0 °C exclude these two types of profiles from the "melting process" and the "supercooled warm rain process", these two mechanisms can explain the formation of WFR by considering the temperature lag between raindrops and atmosphere.

3.4 Real WFR events

The above sensitivity experiments consider ideal temperature profiles, while

real temperature profiles are more complex. To test the applicability of the temperature lag for real WFR events, the theoretical model (section 2.2) is applied to the real conditions for all 25 WFR events observed at the sounding stations over the two decades of the study period.

Figures 10a and 10b represent the profiles of the "melting" and "supercooled warm rain process", respectively. The calculated results of the "melting mechanism" (Figure 10a) show that the ice crystals completely melt into raindrops at the bottom of the melting layer (~2500 m). At that time, T_r is equal to T_a, T_{ar}=0. T_{ar} gradually increases as the raindrop falling distance increases. Since $\Gamma > 0$ in the near-surface layer, T_r of the raindrops falling to the ground is much lower than T_a. Although the $T_a > 0$℃ near the surface, the falling raindrops remain supercooled ($T_r = -0.6$℃) and form WFR when they fall into the warm layer near the surface.

The corresponding profile for the "supercooled warm rain mechanism" (Figure 10b) shows that the initial precipitation particles in the cloud remained supercooled. The air temperature above the near-surface layer was below 0℃. The raindrops maintained a temperature lag of ±0.9 °C with the atmosphere. When the raindrops fell into the warm layer near the surface, the raindrops remained supercooled (T_r=-0.3°C) and formed WFR.

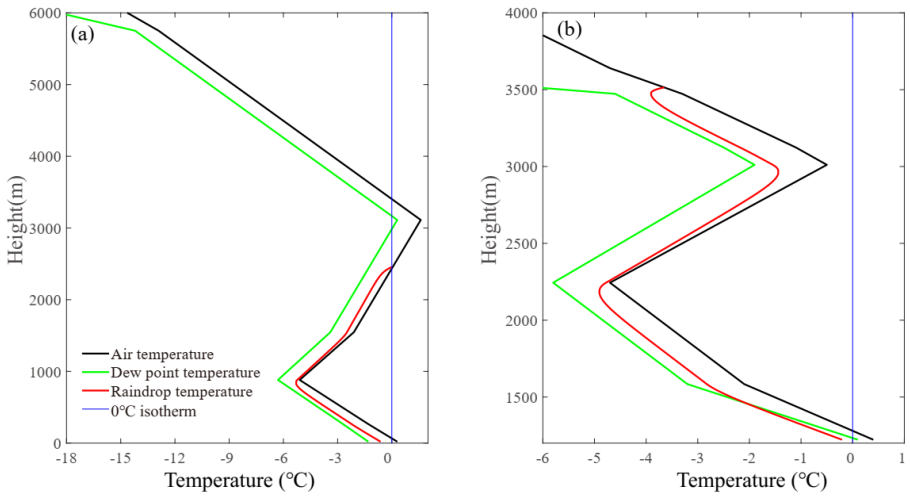

Figure 10. Calculated variation of T_r corresponding to two real WFR profiles (D=2 mm).(a) melting profile that was taken in Guilin(WMO number:57957) at 1200UTC 28th Jan 2008;(b)supercooled warm rain profile that was taken in Guizhou(WMO number:57816) at 00UTC 08th Jan 2018.

The distribution of the calculated T_r and T_a at surface for the 25 WFR events (Figure 11) show that the model captures 15 WFR cases when D=1 mm; When the raindrop diameter increases to 2 mm, the model can accurately diagnose

more than 95% (24 cases) of the WFR events, implying that the initial raindrop diameters in the WFR events were likely equal to or larger than 2 mm

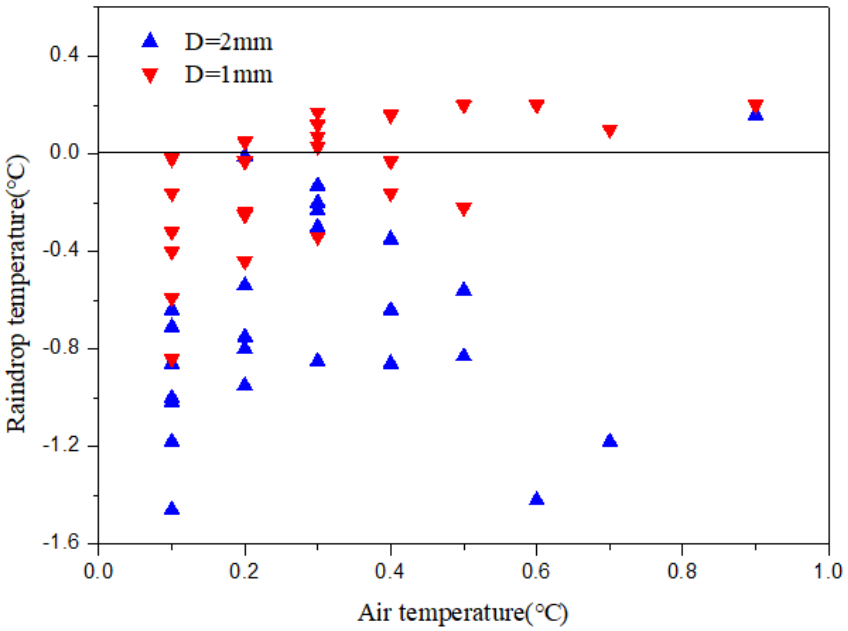

Figure 11. Distribution of the calculated T_{ar} and T_a for the 25 WFR events. (The region below the 0℃ isotherm represents the area where the model accurately diagnoses the WFR events.)

Moreover, the model and sensitivity results can be applied to explain the difference in the frequency of WFR events occurring at different station altitudes as follows.

1 Raindrop size effect: Observations at Nanjing (Wen et al., 2019), Lushan (Huang et al., 2019), and Weining (Zhang et al., 2018) show that the raindrop size distribution is narrow at high-altitude stations for freezing rain events, with the maximum sizes of raindrops is only 1.25 mm and the mean diameters is 0.34mm. In contrast, the raindrop size distributions are significantly wider at low and middle station altitudes (Figure 12). The maximum sizes of raindrops are 4.1/4.25mm and the mean diameters are 0.53/0.65mm low/middle altitudes station respectively. Therefore, the raindrops at high station altitude tend to have smaller sizes than at low and middle station altitudes. According to the sensitivity test, the temperature lag of raindrops increases with increasing D. Therefore, the temperature lag of raindrops at high station altitudes is weaker, which results in a lower probability of WFR events occurring than at low and middle station altitudes.

2 RH effect: The temperature lag of raindrops increases with increasing RH.

Zhang et al. (2018) showed that the mean RH at low-altitude stations is much lower than that at high-altitude stations in winter. Therefore, the temperature lag of raindrops at high station altitudes is smaller than at lower station altitudes, which leads to a lower probability of WFR events at high station altitudes. In addition, the observations (Figure 12) indicate that the number of large raindrops is less than that of small raindrops. Thus, with increasing air temperature, the temperature lag is insufficient to keep the temperature of small raindrops below 0 °C, resulting in a gradual decrease in the frequency of WFR events.

3) Lapse effect: Fig 13 shows the distribution of Γ in the lower atmosphere (0-500m) when freezing rain events occurred at sounding stations in China from 2000 to 2019. There are large differences in the distribution of Γ at different station altitudes. When the station altitude is lower than 1000m, almost all freezing rain events occur at $\Gamma > 0$; when the station altitude is greater than 1000m, nearly 40-50% of the freezing rain events occurred at $\Gamma < 0$. According to the sensitivity test, the temperature lag of raindrops increases with increasing Γ. The Γ values at low altitudes are significantly higher than that at high station altitudes when the freezing rain occurred, implying that the temperature lag of raindrops at high station altitudes is weaker and the probability of WFR events occurring is much less than that at low station altitude.

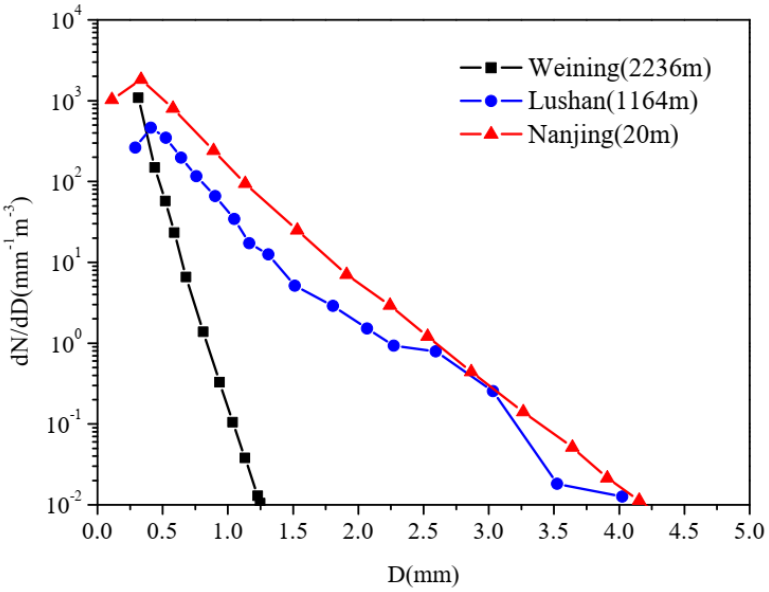

Figure 12. Characteristics of raindrop size distributions in freezing rain events at stations at different altitudes.The data in this figure combines the data from the observational studies by Wen et al.(2019), Huang et al.(2019), and Zhang et al.(2018) .

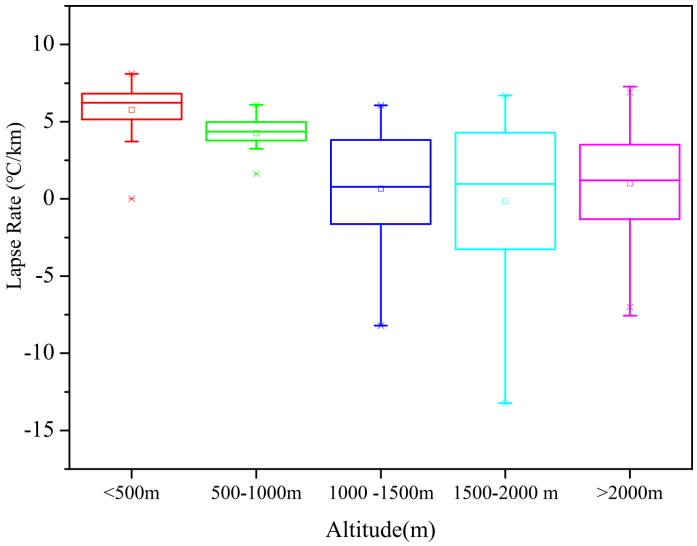

Figure 13. Distributions of the Γ at different station altitudes during freezing rain events.

4 Conclusions

Analysis of 20-year observations across China shows that 656 WFR events occurred, accounting for 7% of the total number of freezing rain events. The WFR occurrence frequency at low-altitude stations is found to be higher than that at high-altitude stations. Moreover, the frequency of freezing rain events gradually decreases as the surface temperature increases, but WFR events may still occur at surface temperatures greater than 1 °C.

Based on the assumption that raindrops cannot maintain an equilibrium state in the real atmosphere, a theoretical model of raindrop temperature is presented by relaxing the equilibrium assumption to consider the transient heat exchange between raindrops and the atmosphere. Sensitivity analysis of the model shows that the T_r is not equal to T_a when raindrops fall, the direction of T_r departure from equilibrium depends on the sign of the temperature lapse rate , and the magnitude of the temperature lag is determined by the raindrop diameter D, , and relative humidity RH. An increase of D, an increase of , and a decrease of RH enhance the lag of raindrop temperature and thus the occurrence of the WFR events.

The temperature lag between raindrops and the atmosphere is the main cause of WFR. The diagnosis results for ideal temperature profiles showed that WFR events can form by the "melting mechanism" or "supercooled warm rain mechanism" when considering the temperature lag between raindrops and the atmosphere. The temperature profiles of WFR have two common features: a cold layer (or sub-freezing layer) above the near-surface layer and Γ >0℃/km in the lower atmosphere.

Smaller raindrop sizes, large RH and Γ at high station altitudes result in weaker temperature lag of raindrops, which leads to less frequent WFR. Conversely, with decreasing station altitudes, the raindrop sizes gradually increase and RH decreases, which results in the high frequency of WFR events.

APPENDIX

Table A1. List of symbols, definitions, and their units found in the text.

Symbol	Definition	Value or Reference	Units
T_r	Raindrop temperature	--	K
T_a	Air temperature	--	K
Q_T	Total heat change of raindrops	--	J
Q_e	Heat change of evaporation	--	J
Q_r	Heat change of convection	--	J
Q_h	Heat change of radiation	--	J
F_h	Ventilation coefficient for heat	Rasmussen and Heymsfield (1987)	--
F_v	Ventilation coefficient for vapour	Rasmussen and Heymsfield (1987)	--
D	Diameter of raindrop	--	m
ρ_w	Density of water	1,000	kg $\cdot$ m^{-3}
C_w	Specific heat capacity of water	4,200	J $\cdot$ kg^{-1} $\cdot$ K^{-1}
L_e	Latent heat of evaporation	2,264	KJ $\cdot$ Kg^{-1}
D_v	Coefficient of diffusion	Hall and Pruppacher (1976)	cm^2 $\cdot$ s^{-1}
R_V^*	Gas constant of vapour	Hall and Pruppacher (1976)	J $\cdot$ K^{-1} $\cdot$ Kg^{-1}
RH	Relative humidity	--	%
e_{sat}	Saturated vapour pressure	Murray (1966)	hPa
K_a	Thermal conductivity of air	Beard and Pruppacher (1971)	J $\cdot$ m^{-1} $\cdot$ s^{-1} $\cdot$ K^{-1}
ε	Coefficient of black-body radiation	0.9	--
σ	Stefan Boltzmann constant	5.67$\times$10^{-8}	W $\cdot$ m^{-2} $\cdot$ K^{-4}
U(D)	raindrop fall velocity	Best(1950); Atlas et al(1973)	cm $\cdot$ s^{-1}
C_1	Empirical coefficient	965	cm $\cdot$ s^{-1}
C_2	Empirical coefficient	1030	cm $\cdot$ s^{-1}
C_3	Empirical coefficient	1200	cm^{-1}

Acknowledgments

This study is supported by the National Natural Science Foundation of China (41875176). Y. Liu is supported by the U.S. Department of Energy's Atmospheric System Research (ASR) program.

Conflict of interest

No conflict of interest exits in the submission of this manuscript, and all authors approve the manuscript for publication. On behalf of my co-authors, I would like to declare that the work described was original research that has not been published previously, and not under consideration for publication elsewhere, in

whole or in part. All the authors listed have approved the manuscript that is enclosed.

Data Availability Statement:

The observational data and code in the study are available at Lu, Zhengqi (2021), "Raindrop temperature model", Mendeley Data, v1, http://dx.doi.org/10.17632/4g9dfkt8y9.1.

References

Abraham, F. F., Jordan, S. K., Kortzeborn, R. N., & Kolsky, H. G. (1972). Model for time-dependent raindrop size distributions; Application to the washout of airborne contaminants. *IBM Journal of Research and Development*, *16*(2), 91-100. https://doi.org/10.1175/BAMS-D-11-00091.1

Adhikari, A., & Liu, C. (2019). Remote sensing properties of freezing rain events from space. *Journal of Geophysical Research: Atmospheres*, *124*(19), 10385-10400. https://doi.org/10.1029/2019JD030788

Andersson, A., & Chapman, L. (2011). The use of a temporal analogue to predict future traffic accidents and winter road conditions in Sweden. *Meteorological Applications*, *18*(2), 125-136. https://doi.org/10.1002/met.186

Anderson, S. P., Hinton, A., & Weller, R. A. (1998). Moored observations of precipitation temperature. Journal of Atmospheric and Oceanic Technology, 15(4), 979-986. https://doi.org/10.1175/1520-0426(1998)015%3c0979:MOOPT%3e2.0.CO;2

Atlas, D., Srivastava, R. C., & Sekhon, R. S. (1973). Doppler radar characteristics of precipitation at vertical incidence. *Reviews of Geophysics*, *11*(1), 1-35. https://doi.org/10.1029/RG011i001p00001

Barszcz, A., Milbrandt, J. A., & Thériault, J. M. (2018). Improving the explicit prediction of freezing rain in a kilometer-scale numerical weather prediction model. *Weather and Forecasting*, *33*(3), 767-782. https://doi.org/10.1175/WAF-D-17-0136.1

Beard, K. V., & Pruppacher, H. R. (1971). A wind tunnel investigation of the rate of evaporation of small water drops falling at terminal velocity in air. *Journal of Atmospheric Sciences*, *28*(8), 1455-1464. https://doi.org/10.1175/1520-0469(1971)028%3c1455:AWTIOT%3e2.0.CO;2

Best, A. C. (1950). Empirical formulae for the terminal velocity of water drops falling through the atmosphere. *Quarterly Journal of the Royal Meteorological Society*, *76*(329), 302-311. https://doi.org/10.1002/qj.49707632905

Caplan, P. M. (1966). On the evaporation of raindrops in the presence of vertical gradients of temperature and relative humidity. *Journal of the Atmospheric Sciences*, *23*(5), 614-617. https://doi.org/10.1175/1520-0469(1966)023%3c0614:OTEORI%3e2.0.CO;2

Carrière, J. M., Lainard, C., Le Bot, C., & Robart, F. (2000). A climatological study of surface freezing precipitation in Europe. *Meteorological Applications,*, *7*(3), 229-238. https://doi.org/10.1017/S1350482700001560

Cholette, M., Thériault, J. M., Milbrandt, J. A., & Morrison, H. (2020). Impacts of predicting the liquid fraction of mixed-phase particles on the simulation of an extreme freezing rain event: the 1998 North American Ice Storm. *Monthly Weather Review*, *148*(9), 3799-3823. https://doi.org/10.1175/MWR-D-20-0026.1

Cortinas Jr, J. V., Bernstein, B. C., Robbins, C. C., & Walter Strapp, J. (2004). An analysis of freezing rain, freezing drizzle, and ice pellets across the United States and Canada: 1976–90. *Weather and Forecasting*, *19*(2), 377-390. https://doi.org/10.1175/1520-0434(2004)019%3c0377:AAOFRF%3e2.0.CO;2

Czys, R. R., Scott, R. W., Tang, K. C., Przybylinski, R. W., & Sabones, M. E. (1996). A physically based, nondimensional parameter for discriminating between locations of freezing rain and ice pellets. *Weather and forecasting*, *11*(4), 591-598. https://doi.org/10.1175/1520-0434(1996)011%3c0591:APBNPF%3e2.0.CO;2

Deng, D., Gao, S., Du, X., & Wu, W. (2012). A diagnostic study of freezing rain over Guizhou, China, in January 2011. *Quarterly Journal of the Royal Meteorological Society*, *138*(666), 1233-1244. https://doi.org/10.1002/qj.981

Dui, W. (1991). The numerical test on evaporation of raindrop beneath cloud [J]. *Acta Meteorologica Sinica*, *1*.

Hindmarsh, J. P., Russell, A. B., & Chen, X. D. (2003). Experimental and numerical analysis of the temperature transition of a suspended freezing water droplet. *International Journal of Heat and Mass Transfer*, *46*(7), 1199-1213. https://doi.org/10.1016/S0017-9310(02)00399-X

Gibson, S. R., & Stewart, R. E. (2007). Observations of ice pellets during a winter storm. *Atmospheric research*, *85*(1), 64-76. https://doi.org/10.1016/j.atmosres.2006.11.004

Hall, W. D., & Pruppacher, H. R. (1976). The survival of ice particles falling from cirrus clouds in subsaturated air. *Journal of Atmospheric Sciences*, *33*(10), 1995-2006. https://doi.org/10.1175/1520-0469(1976)033%3c1995:TSOIPF%3e2.0.CO;2

Hanesiak, J. M., & Stewart, R. E. (1995). The mesoscale and microscale structure of a severe ice pellet storm. *Monthly weather review*, *123*(11), 3144-3162. https://doi.org/10.1175/1520-0493(1995)123%3c3144:TMAMSO%3e2.0.CO;2

Huang, Q., Niu, S. J., Lv, J. J. (2018). Physical Characteristics of Freezing Raindrop Size Distribution and Terminal Velocity in Two Ice Weather Cases in Lushan Area. *Chinese Journal of Atmospheric Sciences*, 2018, 42(5): 1023-1037.

https://doi.org/10.3878/j.issn.1006-9895.1711.17158

Huffman, G. J., & Norman Jr, G. A. (1988). The supercooled warm rain process and the specification of freezing precipitation. *Monthly weather review*, *116*(11), 2172-2182. https://doi.org/10.1175/1520-0493(1988)116%3c2172:TSWRPA%3e2.0.CO;2

Johnson, D. A., & Hallett, J. (1968). Freezing and shattering of supercooled water drops. *Quarterly Journal of the Royal Meteorological Society*, *94*(402), 468-482. https://doi.org/10.1002/qj.49709440204

Khain, A., Rosenfeld, D., Pokrovsky, A., Blahak, U., & Ryzhkov, A. (2011). The role of CCN in precipitation and hail in a mid-latitude storm as seen in simulations using a spectral (bin) microphysics model in a 2D dynamic frame. *Atmospheric Research*, *99*(1), 129-146. https://doi.org/10.1016/j.atmosres.2010.09.015

Kiessling, F., Nefzger, P., Nolasco, J. F., & Kaintzyk, U. (2014). *Overhead power lines: planning, design, construction*. Springer.

Kincaid, D. C., & Longley, T. S. (1989). A water droplet evaporation and temperature model. *Transactions of the ASAE*, *32*(2), 457-0462. https://doi.org/10.13031/2013.31026

Lee, S. S., & Feingold, G. (2010). Precipitating cloud-system response to aerosol perturbations. *Geophysical Research Letters*, *37*(23). https://doi.org/10.1029/2010GL045596

Milbrandt, J. A., & Yau, M. K. (2005). A multimoment bulk microphysics parameterization. Part I: Analysis of the role of the spectral shape parameter. *Journal of the atmospheric sciences*, *62*(9), 3051-3064. https://doi.org/10.1175/JAS3534.1

Morrison, H., & Milbrandt, J. A. (2015). Parameterization of cloud microphysics based on the prediction of bulk ice particle properties. Part I: Scheme description and idealized tests. *Journal of Atmospheric Sciences*, *72*(1), 287-311. https://doi.org/10.1175/JAS-D-14-0065.1

Murray, F. W. (1966). *On the computation of saturation vapor pressure*. Rand Corp Santa Monica Calif.

Nagumo, N., Adachi, A., & Yamauchi, H. (2019). Geometrical properties of hydrometeors during the refreezing process and their effects on dual-polarized radar signals. *Monthly Weather Review*, *147*(5), 1753-1768. https://doi.org/10.1175/MWR-D-18-0278.1

Pruppacher, H. R., & Klett, J. D. (2012). *Microphysics of Clouds and Precipitation: Reprinted 1980*. Springer Science & Business Media.

Rasmussen, R. M., & Heymsfield, A. J. (1987). Melting and shedding of graupel and hail. Part I: Model physics. *Journal of Atmospheric Sciences*, *44*(19), 2754-2763. https://doi.org/10.1175/1520-0469(1987)044%3c2754:MASOGA%3e2.0.CO;2

Rauber, R. M., Ramamurthy, M. K., & Tokay, A. (1994). Synoptic and mesoscale structure of a severe freezing rain event: The St. Valentine's Day ice storm. *Weather and forecasting*, *9*(2), 183-208. https://doi.org/10.1175/1520-0434(1994)009%3c0183:SAMSOA%3e2.0.CO;2

Roberts, E., & Stewart, R. E. (2008). On the occurrence of freezing rain and ice pellets over the eastern Canadian Arctic. *Atmospheric Research*, *89*(1-2), 93-109.

https://doi.org/10.1016/j.atmosres.2007.11.032

Salamalikis, V., Argiriou, A. A., & Dotsika, E. (2016). Isotopic modeling of the sub-cloud evaporation effect in precipitation. *Science of the Total Environment*, *544*, 1059-1072. https://doi.org/10.1016/j.scitotenv.2015.11.072

Sanders, K. J., & Barjenbruch, B. L. (2016). Analysis of ice-to-liquid ratios during freezing rain and the development of an ice accumulation model. *Weather and Forecasting*, *31*(4), 1041-1060. https://doi.org/10.1175/WAF-D-15-0118.1

Stewart, R. E., Thériault, J. M., & Henson, W. (2015). On the characteristics of and processes producing winter precipitation types near 0° C. *Bulletin of the American Meteorological Society*, *96*(4), 623-639. https://doi.org/10.1175/BAMS-D-14-00032.1

Tardif, R., & Rasmussen, R. M. (2010). Evaporation of nonequilibrium raindrops as a fog formation mechanism. *Journal of the atmospheric sciences*, *67*(2), 345-364. https://doi.org/10.1175/2009JAS3149.1

Thériault, J. M., & Stewart, R. E. (2010). A parameterization of the microphysical processes forming many types of winter precipitation. *Journal of the Atmospheric Sciences*, *67*(5), 1492-1508. https://doi.org/10.1175/2009JAS3224.1

Thompson, G., Rasmussen, R. M., & Manning, K. (2004). Explicit forecasts of winter precipitation using an improved bulk microphysics scheme. Part I: Description and sensitivity analysis. *Monthly Weather Review*, *132*(2), 519-542. https://doi.org/10.1175/1520-0493(2004)132%3c0519:EFOWPU%3e2.0.CO;2

Tobin, D. M., & Kumjian, M. R. (2017). Polarimetric radar and surface-based precipitation-type observations of ice pellet to freezing rain transitions. *Weather and Forecasting*, *32*(6), 2065-2082. https://doi.org/10.1175/WAF-D-17-0054.1

Wen, L., Zhao, K., Wang, M., & Zhang, G. (2019). Seasonal variations of observed raindrop size distribution in East China. *Advances in Atmospheric Sciences*, *36*(4), 346-362. https://doi.org/10.1007/s00376-018-8107-5

Zerr, R. J. (1995). Wind and reflectivity signatures as obtained by a Doppler radar for a freezing-rain episode. In *Conference on Radar Meteorology, 27 th, Vail, CO* (p. 1995).

Zhang, Y., Zhang, L., Guo, J., Feng, J., Cao, L., Wang, Y., & Liu, H. (2018). Climatology of cloud-base height from long-term radiosonde measurements in

China. *Advances in Atmospheric Sciences*, *35*(2), 158-168. https://doi.org/10.1007/s00376-017-7096-0

Zhang, Z., Han, Y. X., Wang, J., & Liu, C. R. (2016). Microphysics characteristics and causes of freezing precipitation in mountainous area over Yunnan-Guizhou Plateau. *Journal of the Meteorological Sciences*, *36*(3), 389-395.

Zhao, L. N., Ma, Q. Y., Yang, G. M., Wang, X. R., Zhao, L. Q., Yang, X. D., & Mao, D. Y. (2008). Disasters and its impact of a severe snow storm and freezing rain over southern China in January 2008. *Climatic and Environmental Research*, *13*(4), 556-566.

Zhou, S. H. (2000). Quality control and technical method for producing data set for upper-air in China. Journal of Applied Meteorological Science (in Chinese), 03:109-115.

Zhou, Y., Yue, Y., Gao, Z., & Zhou, Y. (2017). Climatic Characteristics and Determination Method for Freezing Rain in China. *Advances in Meteorology*, *2017*. https://doi.org/10.1155/2017/4635280